Mechanical Systems and Signal Processing 70-71 (2016) 161–175

Contents lists available at ScienceDirect

Mechanical Systems and Signal Processing

journal homepage: www.elsevier.com/locate/ymssp

Autocorrelation-based time synchronous averaging for condition monitoring of planetary gearboxes in wind turbines

Jong M. Ha [a], Byeng D. Youn [a,*], Hyunseok Oh [b], Bongtae Han [b], Yoongho Jung [c], Jungho Park [a]

[a] Department of Mechanical and Aerospace Engineering, Seoul National University, Seoul 151-742, Republic of Korea
[b] Department of Mechanical Engineering, University of Maryland, College Park, MD 20742, USA
[c] School of Mechanical Engineering, Pusan National University, Pusan 609-735, Republic of Korea

ARTICLE INFO

Article history:
Received 18 September 2014
Received in revised form
28 April 2015
Accepted 27 September 2015
Available online 23 October 2015

Keywords:
Wind turbine
Planetary gearbox
Condition monitoring
Signal isolation
Time synchronous averaging (TSA)

ABSTRACT

We propose autocorrelation-based time synchronous averaging (ATSA) to cope with the challenges associated with the current practice of time synchronous averaging (TSA) for planet gears in planetary gearboxes of wind turbine (WT). An autocorrelation function that represents physical interactions between the ring, sun, and planet gears in the gearbox is utilized to define the optimal shape and range of the window function for TSA using actual kinetic responses. The proposed ATSA offers two distinctive features: (1) data-efficient TSA processing and (2) prevention of signal distortion during the TSA process. It is thus expected that an order analysis with the ATSA signals significantly improves the efficiency and accuracy in fault diagnostics of planet gears in planetary gearboxes. Two case studies are presented to demonstrate the effectiveness of the proposed method: an analytical signal from a simulation and a signal measured from a 2 kW WT testbed. It can be concluded from the results that the proposed method outperforms conventional TSA methods in condition monitoring of the planetary gearbox when the amount of available stationary data is limited.

1. Introduction

Condition monitoring has been widely implemented to reduce the operation and maintenance costs of wind turbines (WTs) [1]. One of the most critical components of WTs for condition monitoring is the gearbox since unexpected failure of gearboxes leads to high downtime loss [2]. Diagnostics of gearboxes, however, is challenging for several reasons. First, the signals from faulty gears are mixed with those from noisy sources around the gearbox such as bearings. For accurate diagnostics, vibration produced by a gear should be isolated from the mixed vibration signal. Second, vibration signals from healthy and/or faulty gears are mostly non-stationary, because wind speed—and thus the gear speed—rapidly varies over time. Various time–frequency analysis methods can serve as diagnostics tools for non-stationary signals [3]; however, they are too computationally expensive to be used in real-time condition monitoring. Third, the supervisory control and data acquisition (SCADA) and/or the condition monitoring system (CMS) generate a substantially large amount of sensory data

* Corresponding author. Tel.: +82 2 880 1664.
E-mail address: bdyoun@snu.ac.kr (B.D. Youn).

http://dx.doi.org/10.1016/j.ymssp.2015.09.040
0888-3270/

Nomenclature

f_{rev}	resampling frequency (number of samples per revolution)
f_{HTC}	number of samples per hunting tooth cycle (*HTC*)
N_p	number of teeth of the planet gear
N_r	number of teeth of the ring gear
n_{pr}	number of rotations of the planet gear relative to the ring gear
n_c	number of rotations of the carrier
w_c	rotational speed of the carrier (rev/s)
T_r	tooth sequence of the ring gear
T_p	tooth sequence of the planet gear
v_{rs}	resampled vibration signal
v_{win}	windowed vibration signal
$v_i(\theta)$	ith segment corresponding to ith rotation of the gear of interest averaged for TSA
M_p	meshing teeth matrix of the planet gear
M_r	meshing teeth matrix of the planet gear
HTR_p	hunting tooth ratio in terms of rotation of the planet gear
P	number of planet gears
$R_{vv(i)}$	autocorrelation function during ith *HTC*
$\overline{R_{vv}}$	representative autocorrelation function
n_{near}	number of rotations of the planet gear at which the planet gear of interest is near the sensor
D_{max}	maximum distance of the planet gear to the sensor
v_{trans}	transformed vibration signal
W_{trans}	transformed window function
$v_{(i,k)}$	kth teeth meshing vibration vector of tooth number i of the planet gear
$W_{(i,k)}$	kth window vector of tooth number i of the planet gear
$A(f_1)$	amplitude of the ith harmonic of the gear meshing frequency
$A(f_{s(i)})$	amplitude of the ith sidebands on each side of fundamental gear meshing frequency
$RES(i)$	ith sample of the residual signal
$DIF(i)$	ith sample of the difference signal
v_a	analytic vibration signal
v_p	vibration from ith planet gear
a_{pi}	transfer factor from the ith planet gear
HTC	hunting tooth cycle representing the number of full cycles of HTR

for diagnostics of WTs [4]. This large amount of data gives rise to challenges in data acquisition, data transmission, signature extraction, sensor network design, etc.

Time synchronous averaging (TSA) is known to be efficient in the diagnostics of gearboxes [5,6]. TSA can isolate a vibration signal of a particular component from noisy sensory signals. McFadden et al. [7] utilized TSA with a narrow-range rectangular window to isolate the vibration of planet gears. The narrow window function filtered out noisy signals from the sensor data effectively as a planet gear of interest was located adjacent to sensors. The use of a narrow-range Hann window with a smooth edge was also proposed since the rectangular shape of the window led to discontinuity of the extracted signal [8]. Later Samuel et al. [9] suggested a narrow-range Tukey window with a flat-shaped top after realizing that a narrow-range Hann window could also undesirably deform the vibration signal due to its non-flat top nature.

Although they can reduce noise in vibration signals effectively, TSA with such narrow-range window functions require extensive stationary vibration signals. In practice, it is difficult to collect the amount of data because stationary signal is rarely obtainable under the actual operating conditions of WTs. It was reported that the rated operation of WTs, which can cause stationary vibration signals, only accounts for about 19% of operating time [10]. This means that the range of the window functions should be extended to fully utilize the rarely obtainable stationary vibration signals for TSA. As an alternative, a full-range cosine window that utilized the entire range of signals was employed [11]. It was reported, however, that such a full-range window could distort the vibration signal [9]. Thus, it is imperative to design a new wider-range window that optimizes shape and range to maximize the performance of TSA while preventing distortion of the vibration signal.

We propose autocorrelation-based time synchronous averaging (ATSA) to cope with the aforementioned challenges associated with the current practice of TSA for gearboxes. In the proposed approach, an autocorrelation function, which represents physical interactions between the ring, sun, and planet gears in the gearbox, defines optimum windows using actual kinetic responses, thereby preventing distortion of the signal during the TSA process. An order analysis with the ATSA signals makes accurate real-time diagnostics of planetary gearboxes practical. The TSA for diagnostics of a planet gear is reviewed in Section 2. The proposed method is described in Section 3. In Section 4, two case studies are presented to demonstrate the effectiveness of the proposed method.

2. Background: time synchronous averaging for planetary gearbox in wind turbines

TSA is used, among other applications, to isolate the vibration signal produced by a particular gear of interest from noisy sensory signal for efficient condition monitoring of the gear [5]. Although various signal-processing methods have been developed to enhance the performance of TSA, there is room for further improvement to make it directly applicable for fault

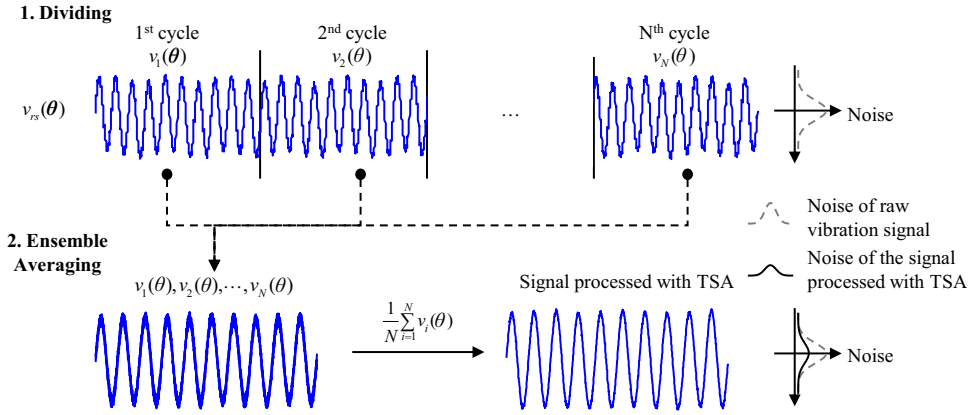

Fig. 1. Procedures of conventional TSA.

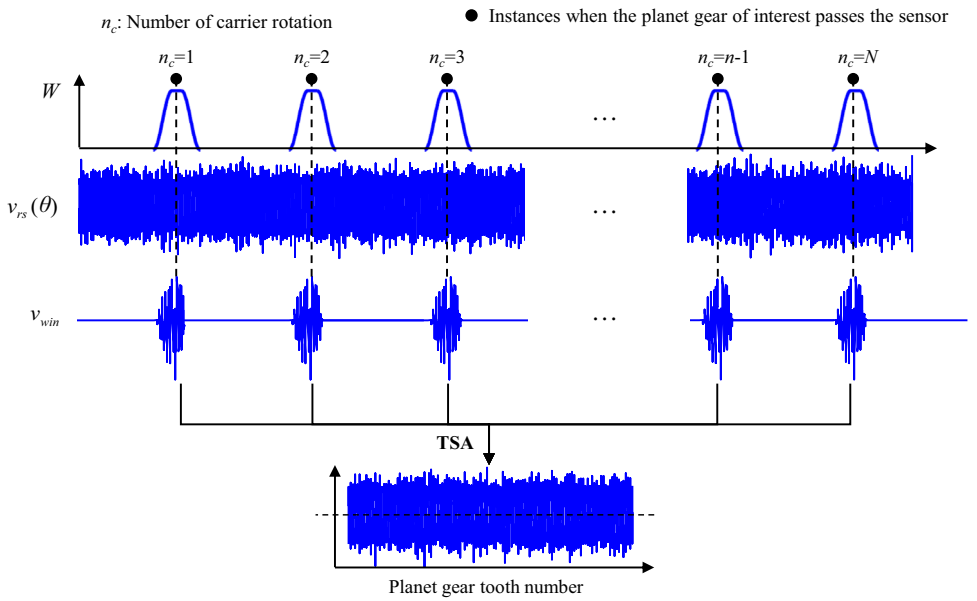

Fig. 2. Isolation of planet gear's vibration using TSA with window function.

diagnostics of planetary gearboxes in WTs. This section provides an overview of TSA for use with planetary gearboxes, and addresses their limitations to be used for wind turbines.

2.1. TSA for planetary gearbox

The conventional TSA divides the sensory signal into *N* segments based on the rotational frequency of the gear of interest, and takes ensemble average for the divided segments as shown in Fig. 1. It is worth noting that vibration signals are collected with a pre-determined sampling rate but the system operates with a varying rotational speed in practice. As a result, the divided segments in Fig. 1 may have the different number of samples. For TSA, thus, the vibration signals should be resampled so that the number of samples assigned during a single revolution of the gear remains constant [12]. This can be achieved by interpolating the vibration signal with the constant angle interval of the consecutive samples. With TSA, vibration signal produced by the gear of interest remains in its own shape because every divided segment contains similar vibration patterns created by meshing of the gear of interest. On the other hand, noise term converges to zero as a considerable number of segments accumulates as shown in right side of Fig. 1.

Numerous attempts have been made to advance the conventional TSA methods for use with planetary gearbox which has four main components, including a carrier, a ring gear, a sun gear, and multiple planet gears. The ring gear is fixed on the gearbox housing and every planet gear rotates together while sharing the load. Unlike spur gears, the axis of the planet gear rotates, as forced by the carrier. Thus, the relative distance of the planet gear from the fixed sensor varies with the rotation of the gears, which leads to challenge in using conventional TSA methods for planetary gearbox.

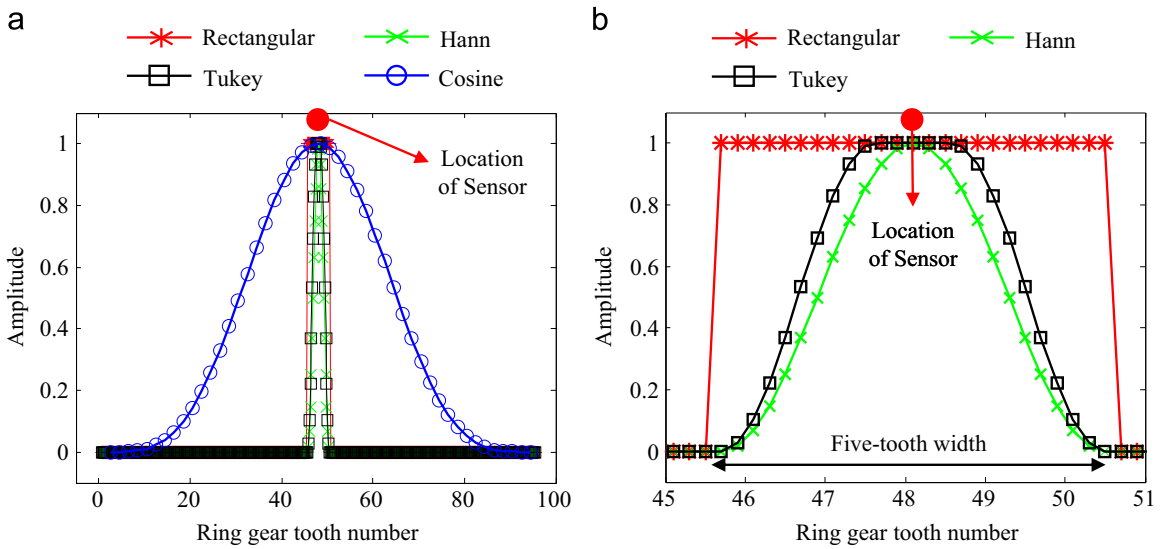

Fig. 3. Representative window functions for TSA: (a) full range view and (b) narrow range view.

Table 1
Performance comparison[a] of TSAs with different windows.

Reference	Window type	Carrier cycles	Required operation time of WT (min)
[7]	Rectangular	1024	51
[15]	Hann	700	35

[a] A wind turbine which operates in 20 rpm of the carrier at its maximum is considered.

McFadden [7] reported that the shorter the relative distance from the sensor to the planet gear of interest, the more accurately the vibration signal of the gear can be measured. Vibration produced by the planet gear of interest, thus, can be monitored by acquiring vibration signals only when the relative distance of the gear from the sensor is short. This is achieved by using window functions that have values only when the planet gear of interest passes the sensor, which is denoted as W in Fig. 2. A windowed signal (v_{win}) can be defined

$$v_{win} = v_{rs}(\theta) \times W \tag{1}$$

where $v_{rs}(\theta)$ is the resampled vibration signal with f_{rev} samples per planet gear's rotation.

Because planet gear tooth numbers that correspond to the windowed signal can be identified by operating characteristics of the planetary gearbox, TSA can be performed by transforming the windowed signals to the planet gears' tooth domain and averaging them as illustrated in Fig. 2.

There are four types of representative window functions for TSA; narrow-range rectangular window [7,13,14], narrow-range Hann window [8,15], narrow-range Tukey window [9,16] and full-range cosine window [11,17]. Fig. 3 compares four types of window functions where it is assumed that the sensor is fixed on tooth number 48 of the ring gear with 95 teeth. The cosine window was normalized to have one at its maximum for convenient comparison of the windows.

2.2. Challenges in using TSA for planetary gearboxes in wind turbines

The applicability of TSA for gearboxes in wind turbines (WTs) is limited in some circumstances including the cases of (1) varying rotational speeds and (2) slow rotational speeds with long time histories, where the assumption of stationarity in vibration data may not be valid. Therefore, it is desired to perform TSA when WTs operate in rated operating conditions under which the gearbox operates with a nominally rated and constant speed, thus resulting in stationary vibration signals. TSA with a narrow-range window function (e.g. Hann, Tukey and rectangular windows) works effectively when a rich amount of vibration data under the rated operation of WTs is available. However, in actual applications, especially for gearboxes in WTs, TSA with narrow-range window functions may not be feasible. Table 1 summarizes the number of carrier cycles used in previous research papers for TSA, and the required the rated operation time for the given WT to generate this number of carrier cycles with the stationary condition. What the table makes clear at once is that TSA with a narrow-range window is not feasible for planetary gearboxes in WTs because the acquisition of stationary vibration data under the rated operation for 35 min with nominally constant speed is unlikely to be achieved.

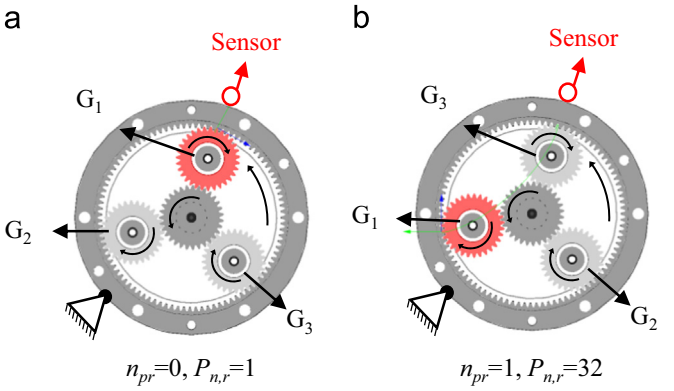

Fig. 4. Position of planet gears where the planet gear of interest is denoted as G1: (a) planet gear of interest is positioned under the sensor and (b) planet gear of interest is positioned far from the sensor.

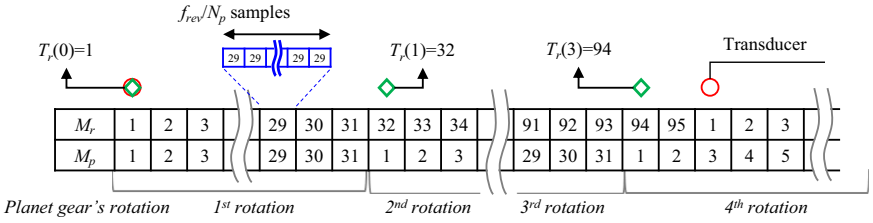

Fig. 5. Meshing tooth matrix of the planet gear and the ring gear.

Although TSA with a full-range window function (e.g., cosine window) may serve as an alternative method because it utilizes the entire range of signals without any loss of data, previous studies pointed out that TSA with such a full-range window function can distort the vibration signal of interest [9,16]. Fig. 4 illustrates an example case to explain how this undesirable distortion occurs by investigating position of the planet gears. When the planet gear of interest is positioned under the sensor (Fig. 4(a)), signal of interest is effectively captured by the sensor. As the planetary gearbox operates, planet gear of interest recedes from the sensor, whereas another planet gear (G_3) approaches the sensor. After one rotation of the planet gear (Fig. 4(b)), G_3 is located almost under the sensor, which means that vibration produced by G_3 dominates the sensory data. Full-range window function takes an entire range of sensory data into account for TSA regardless of the fact that a significant portion of sensory data are dominated by the other planet gears which are out of interest. For condition monitoring of a particular planet gear in the gearbox, vibration signals from other planet gears which are out of interest may serve as a noise. Although the full-range window function gives a small weight when the planet gear of interest is far from the sensor, it is more reasonable to exclude the signals when it is clear that the sensory data is mainly dominated by vibration from the other gears.

3. Autocorrelation-based time synchronous averaging

For efficient TSA, it is extremely important to design a wider range of window function while excluding a substantial portion of sensory data which are out of interest. However, excessive extension of the window range can lead to distortion of the signal. Thus, a wider range of window function is designed to extract the vibration signal of interest while at the same time preventing distortion of signals by considering actual kinetic responses of the gearbox. The work outlined in this paper used a planetary gearbox with a ring gear with 95 teeth and a planet gear with 31 teeth for description of the proposed TSA method.

3.1. Monitoring position and meshing tooth of planet gears

For TSA of vibration signals measured from a planetary gearbox, position and meshing tooth of the gears should be tracked during the operation of the gearbox with an encoder. This can be achieved by accumulating meshing tooth information in a matrix form, which in this paper is called the *meshing tooth matrix* of the ring gear (M_r) and the planet gear (M_p). For identifying meshing tooth information, tooth numbers were pre-assigned to the inner gears of the planetary gearbox in meshing order. Suppose that the tooth of a planet gear of interest indicated by "1" was positioned under the sensor meshing with the tooth of the ring gear indicated by "1" at the initial state. The *meshing tooth matrix* of the ring gear and the planet

gear starts from the number "1", and this value continues to be recorded for f_{rev}/N_p samples which correspond to the number of samples assigned during one-tooth meshing of the gear. As the next tooth of the gear begins to contact the ring gear, number "2" is accumulated in the M_r and M_p. After one rotation of the planet gear, M_p resets to "1" while M_r continues to record the next tooth number because typically the number of teeth of the ring gear is larger than the number of teeth of the planet gear. Fig. 5 shows an example of the *meshing tooth matrix* where a ring gear with 95 teeth and a planet gear with 31 teeth were used.

On the other hand, tooth number of the ring gear that meshes with the planet gear at the n_{pr} rotation can directly be identified by *tooth sequence* of the ring gear (T_r). The concept above can be defined mathematically by the following expression:

$$T_r(n_{pr}) = mod(n_{pr}N_p, N_r) + 1 \tag{2}$$

where

$mod(a,b)$ is the remainder of a/b, n_{pr} is the number of rotations of the planet gear relative to the ring gear, and N_p and N_r are the number of teeth of the planet gear and of the ring gear, respectively.

Using *meshing tooth matrix* and *tooth sequence*, the position and the meshing tooth information of the planet gear of interest can be identified during the operation of the gearbox.

3.2. In-depth study on the autocorrelation function for vibration signals

The autocorrelation function quantifies similarity between shape of the vibration signal at a current time and shape of the vibration signal after a typical time lag (τ) as

$$R_{vv}(\tau) = E[v_{rs}(t)v_{rs}(t+\tau)] \tag{3}$$

where $E[\bullet]$ is the expectation operator, $v_{rs}(t)$ is the resampled vibration signal, and τ is the time lag.

When the time lag is zero, the autocorrelation becomes maximum with two identical signals, say $v(t)$, because of the same vibration pattern. Except for this special condition, autocorrelation is always equal to or smaller than the maximum. When the vibration signal after a typical time lag (τ) has no similar vibration pattern to the original vibration signal due to a different meshing condition (i.e., small similarity), the autocorrelation will give a small value. In the case of TSA for planetary gearboxes, similarity of the segments is not guaranteed because the meshing condition varies as the axes of the planet gears rotate. If one of the segments has no similarity, it should be excluded from the segments averaged by TSA. Thus, the range of the window function can be extended until 'similarity' of the extracted signal is assured.

Fig. 6 shows an example of the autocorrelation function of vibration signals from a sensor that is attached to the top of the planetary gearbox in which ring gear with 95 teeth and three planet gears with 31 teeth are in mesh. As can be seen from the figure, the locally maximum autocorrelation values are observed when the rotation of the planet gear (n_{pr}) is at the particular integer numbers (e.g., 3, 6, 9, etc.), primarily at the interval of three.

Fig. 7 explains how those peaks occur in the autocorrelation function. Suppose that the planet gear of interest is located under the sensor at the initial state. As the gearbox operates, the planet gear of interest starts to recede from the sensor, and vibration excited by the other gears and external sources begins to dominate the vibration signal measured from the sensor.

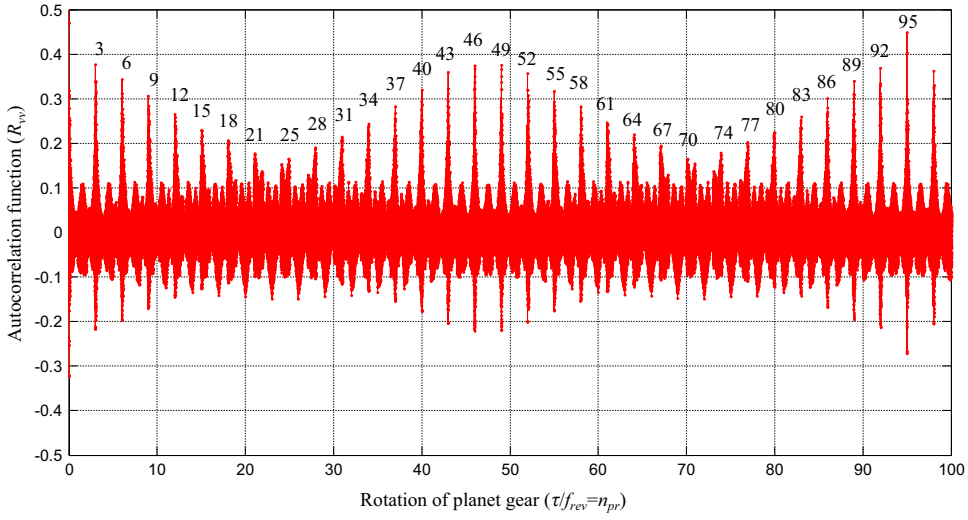

Fig. 6. Autocorrelation function of vibration measured from a sensor attached to a gearbox housing.

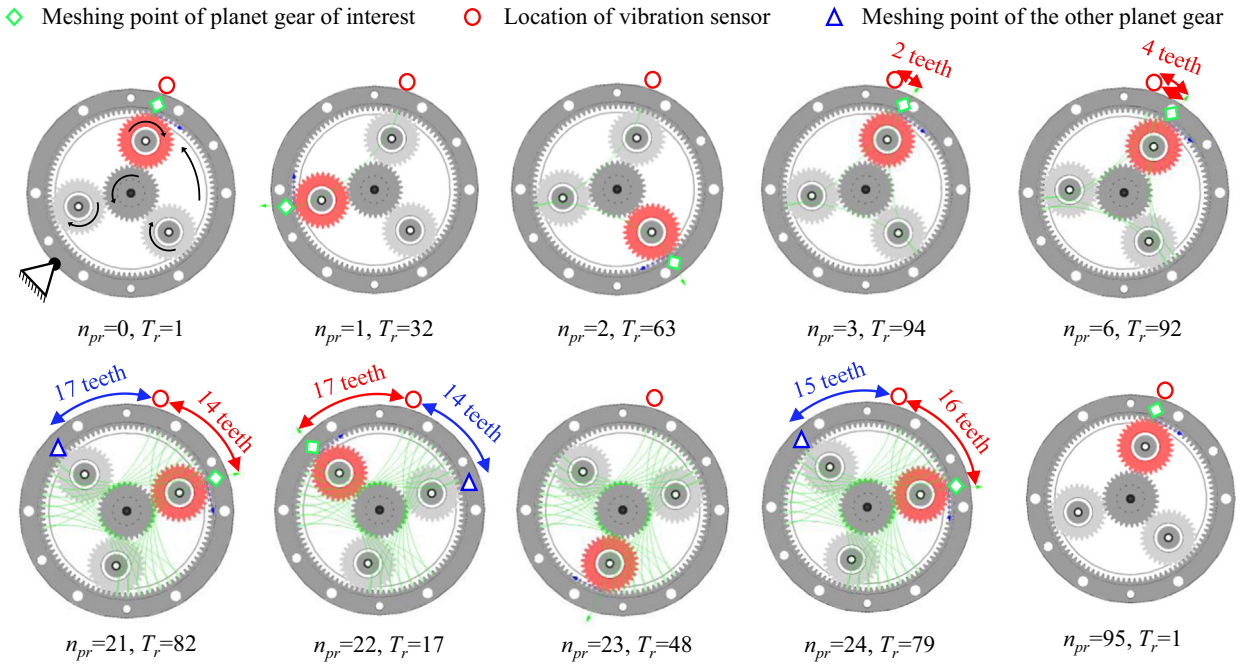

Fig. 7. Meshing condition and transfer path along with rotation of planet gear.

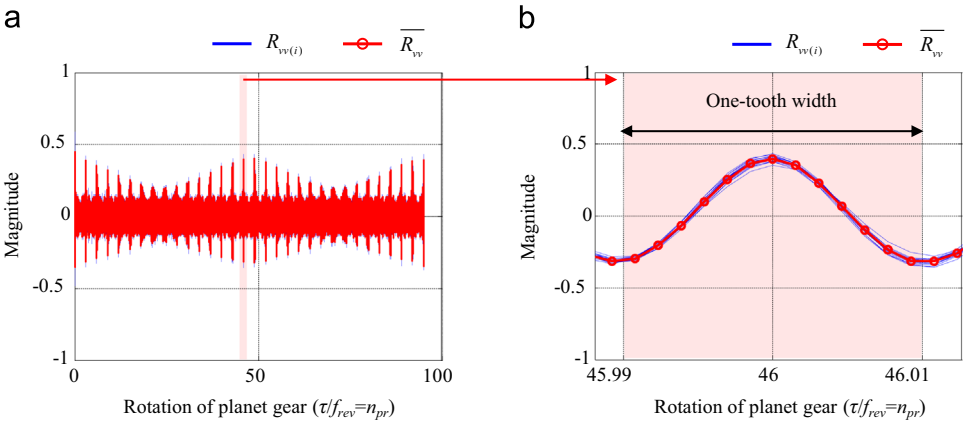

Fig. 8. Representative autocorrelation function: (a) for 1 HTC and (b) for the period of one-tooth meshing around 46 rotations of the planet gear.

This situation will give a small autocorrelation value by a small degree of similarity. The relative distance of the planet gear becomes short again after having three or six additional rotations of the planet gear (n_{pr}=3 or n_{pr}=6). Because vibration from the planet gear of interest dominates the sensor data again at those moments, the sensor measures signals with a similar vibration pattern to the origin. The autocorrelation function, thus, has high peaks at n_{pr}=3 or n_{pr}=6. As a gearbox continues to run, the inner gears resets to the initial condition after a particular rotation of the planet gear. The hunting tooth ratio of the planet gear (HTR_p) is defined as the minimum rotation of the planet gear needed to reset to its initial condition [9]:

$$HTR_p = \frac{LCM(N_p, N_r)}{N_p} \tag{4}$$

where $LCM(a,b)$ is the least common multiple of a and b.

The example case employs the planetary gearbox with an HTR_p of 95. After 95 rotations of the planet gear (n_{pr}=95), the vibration signal measured from the sensor should show the maximum similarity to the original signal because of the identical meshing condition. As predicted, it is found from Fig. 6 that the autocorrelation function has a high peak at n_{pr}=95.

From these observations, it is concluded that the similarity of the time-lagged vibration signal is guaranteed when the relative distance of the planet gear from the sensor is short. Consequently, the range of the window function can be

extended until the relative distance of the planet gear from the sensor is shorter than that of the other gears. Moreover, the autocorrelation function can help define the shape of the window function because the degree of similarity of the vibration signal was quantitatively modeled by the autocorrelation function. In other words, the newly designed window function gives a large weight when the similarity is guaranteed quite well, while it assigns a small weight when a small amount of similarity is assured. As a result, the proposed scheme enables to effectively isolate vibration signals produced by the planet gear of interest while minimizing interference of the other gears which are out of interest by considering actual kinetic responses of the gearbox.

3.3. Representative autocorrelation function

As the gearbox operates, there are a number of chances to reproduce the initial meshing condition as the rotations of the planet gears reach multiples of the HTR_p. For every full cycle of the HTR_p, thus, the repetitive pattern of the autocorrelation function reappears. The autocorrelation function during the ith full cycles of the HTR_p can be defined as

$$R_{vv(i)}(\tau) = E\left[v_{rs}\left(t-(i-1)f_{HTC}\right)v_{rs}\left(t-(i-1)f_{HTC}+\tau\right)\right] \tag{5}$$

where HTC is the hunting tooth cycle representing the number of full cycles of HTR and f_{HTC} is the number of samples per HTC.

A representative autocorrelation function is defined as the ensemble average of the multiple sets of autocorrelation functions as illustrated in Fig. 8.

$$\overline{R_{vv}}(\tau) = \frac{1}{N_{HTC}}\sum_{i=1}^{N_{HTC}} R_{vv(i)}(\tau) \tag{6}$$

where N_{HTC} is the number of hunting tooth cycles ($HTCs$) of the entire signal.

3.4. Design of the autocorrelation-based window

The range and shape of the autocorrelation-based window are defined in this section. First, the range of the window function is defined to extract the vibration signal only when the planet gear of interest is nearer than the other gears to the sensor. Second, the shape of the window function is defined by considering the degree of similarity. When a high level of similarity is assured, the window function will have a high value to assign a large weight in extraction. Because similarity is quantitatively measured by the autocorrelation function, the shape of the window is derived by extracting the representative autocorrelation values where the planet gear of interest is nearest the sensor.

The number of planet gears' rotations at which the planet gear of interest is nearest the sensor can be identified by deducing it from a tooth sequence as

$$T_r(n_{near}) \le D_{max}+1 \quad \text{or} \quad T_r(n_{near}) \ge N_r+1-D_{max} \tag{7}$$

where n_{near} is the number of rotations of the planet gear meshing with the ring gear nearest the sensor and D_{max} is the maximum distance of the planet gear to the sensor.

The maximum distance of the planet gear to the sensor (D_{max}) can be determined in the ring gear's domain to guarantee the range of 'nearest'. Because the ring gear can be divided into $2P$ regions based on the location of the P planet gears, D_{max} is defined as Eq. (8). For example, D_{max} of a planetary gearbox with three planet gears and a ring gear with 95 teeth is described in Fig. 9.

$$D_{max} = floor\left(\frac{N_r}{2P}\right) \tag{8}$$

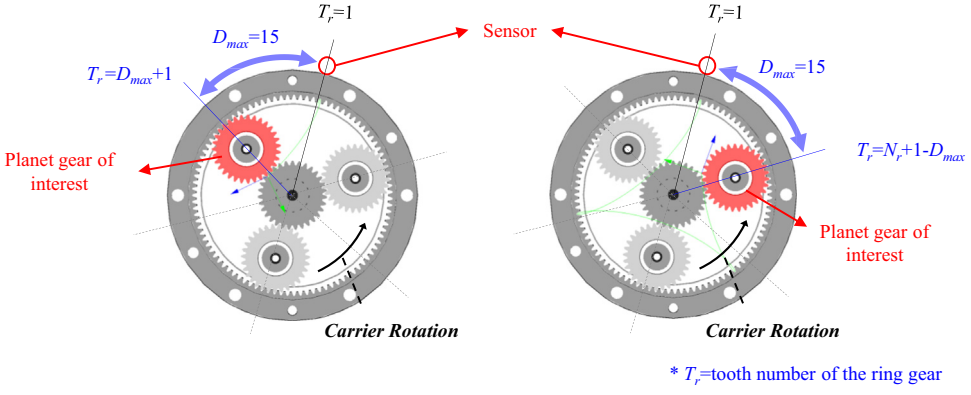

Fig. 9. Maximum distance of the planet gear of interest to the sensor and corresponding position of the gears.

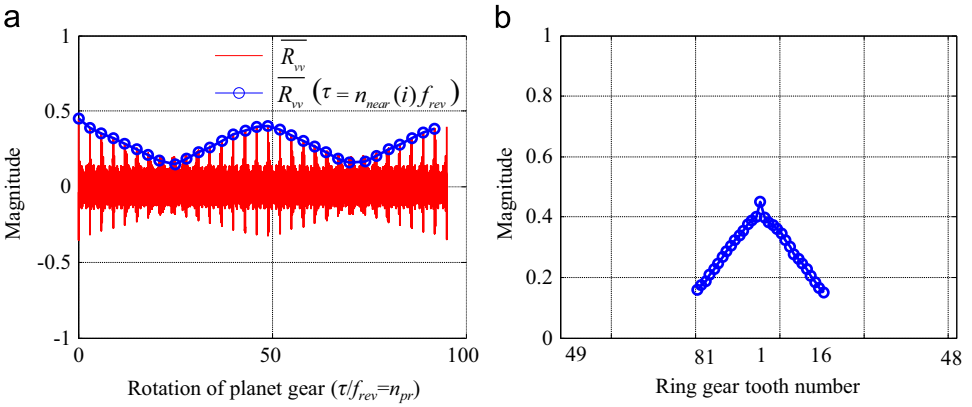

Fig. 10. Derivation of the window function based on representative autocorrelation function: (a) extraction of window function and (b) window function along with ring gears' tooth. (For interpretation of the references to color in this figure legend, the reader is referred to the web version of this article.)

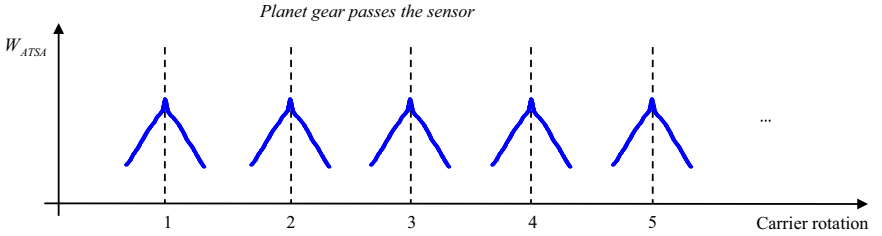

Fig. 11. Autocorrelation-based window function.

where *floor*(a) rounds the value 'a' to the nearest integer less than or equal to a, N_r is the number of teeth of the ring gear, and P is the number of planet gears.

The representative autocorrelation values satisfying Eq. (7) are marked as blue circles in Fig. 10(a). For design of the window function, the extracted autocorrelation values are transformed to the ring gears' tooth domain as shown in Fig. 10 (b). Then, the autocorrelation-based window defined in the entire range of the signal (W_{ATSA}) can be constructed as shown in Fig. 11. Every local window has its center as the planet gear of interest passes the sensor periodically in the carrier rotation.

3.5. Windowing, transforming, and averaging over the ensemble of signals

General procedures of TSA, such as windowing, transforming, and averaging, are followed to process ATSA signals. These procedures are illustrated in Fig. 12. In windowing, the resampled vibration signal (v_{re}) is multiplied by the autocorrelation-based window (W_{ATSA}) to get the windowed signal (v_{win}). The windowed signal is then re-arranged to the planet gear's tooth domain through a transforming step. The *meshing tooth matrix* helps find which tooth of the planet gear produces the windowed signals. When tooth number i of the planet gear is of interest to the TSA, f_{rev}/N_p samples corresponding to the number of samples assigned during one-tooth meshing of the gear can be found by searching i in the *meshing tooth matrix* of the planet gear (M_p). The kth tooth meshing vibration vector of tooth number i of the planet gear is denoted as $v_{(i,k)}$. Fig. 12 illustrates the tooth meshing vibration vectors of tooth number one as an example. Then, the transformed vibration signal corresponding to tooth number i of the planet gear, which is denoted as v_{trans}, can be defined as

$$v_{trans}\left((i-1)\cdot\frac{f_{rev}}{N_p}+1:i\cdot\frac{f_{rev}}{N_p}\right)=\sum\nolimits_k v_{(i,k)} \tag{9}$$

During windowing, the vibration signals are deformed by the non-unity shape of the windows. Moreover, the summation of the windowed signals produces undesirable modulation of the signal. To remove the undesirable modulation of the signal, the pure effect of modulation should be identified. For this purpose, all procedures for defining a transformed vibration signal are performed by applying the constant function with the magnitude of one on behalf of the vibration signal, which results in a transformed window signal (W_{trans}). Transformed window signal corresponding to tooth number i of the planet gear can be defined as

$$W_{trans}\left((i-1)\cdot\frac{f_{rev}}{N_p}+1:i\cdot\frac{f_{rev}}{N_p}\right)=\sum_k W_{(i,k)} \tag{10}$$

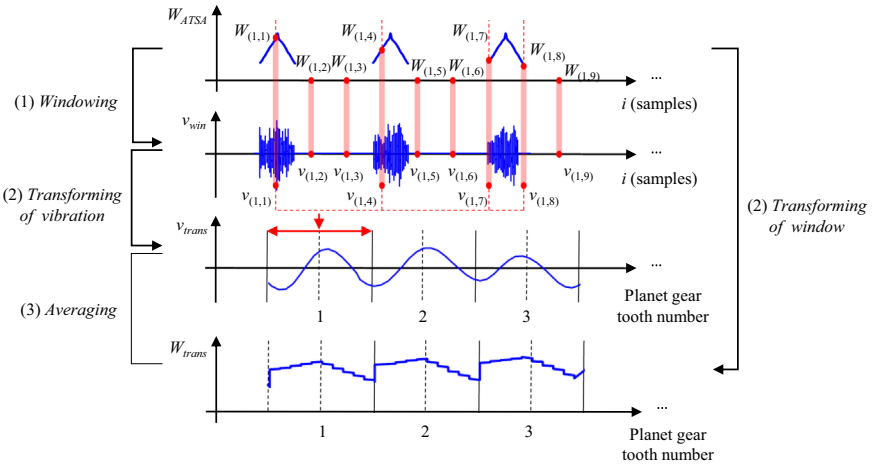

Fig. 12. Averaging of signal for ATSA.

where $W_{(i,k)}$ is extracted from the window function as tooth number i of the planet gear mesh with the ring gear for the kth time. In Fig. 12, $W_{(i,k)}$ that corresponds to tooth number i of the planet gear is illustrated as an example.

If there is no modulation effect, the transformed window function should have a unit value. However, as shown in Fig. 12, the transformed window signal (W_{trans}) is varying, which represents the pure effect of the undesirable modulation. To remove this undesirable effect, the ATSA signal can be defined by dividing the transformed vibration signal by the transformed window.

3.6. Extraction of health indicators

In general, for the purposes of gearbox diagnostics, the residual signal (*RES*) and the difference signal (*DIF*) are obtained from the TSA signals rather than solely using the unmodified TSA signal [18]. *RES* is calculated by removing the fundamental gear meshing frequency (GMF) and its harmonics from the TSA signal so that it contains sideband signals [19]. Because the energy contained in the sidebands is related to failures in the gearbox, statistical moments of the *RES* can be used as a health indicator of gearboxes [20]. *DIF* is obtained from *TSA* by excluding sidebands as well as the fundamental GMF and its harmonics. Ideally *DIF* should not contain any normal vibration components because there are no primary vibration sources, i.e., vibration due to gear dynamics. Hence, *DIF* should follow a Gaussian distribution with a mean of zero (i.e., Gaussian noise) [18]. As the faults in a gear worsen, however, the magnitude of vibration with unexpected frequencies which are out of normal vibration components could become large which would lead to an increase in *DIF*. *DIF* is more sensitive to these changes compared to *RES* because rise in any unexpected frequency in vibration will be the only vibration component in *DIF* whereas RES is dominated by vibration from the sidebands. For this reason, it is useful to track the shape and energy of *DIF* to identify the fault of the gearbox.

There are a number of health indicators exploiting *RES* and *DIF* to perform diagnostics of the gears. Health indicators (HIs) are basically the representative values of *TSA*, *RES* and *DIF*. For example, a statistical moment for *TSA*, *RES* and *DIF* (e.g. mean of *TSA*, *RES* and *DIF*) can be used as three HIs for fault diagnostics of the gearbox. Among various HIs, three kinds of HIs, which are sideband energy ratio (*SER*) [21], *FM4* [22], and *M4* [20] performed best at identifying condition of the gears while representing physical meanings. Thus, the work described in this paper attempts to present discussion on effectiveness of the TSA and ATSA with only *SER*, *FM4* and *M4*. SER represents the amplitudes of sidebands normalized by their fundamental gear meshing frequency (GMF). When a fault occurs in a gear, SER will deviate from the normal boundary because the amplitudes of the sidebands relative to the amplitude of the fundamental GMF are expected to increase. FM4 is the normalized forth moment of DIF, which is sensitive to higher order sidebands generated from unexpected peaks of the signal. M4 is the fourth moment of RES, which can rise when the energy of sidebands increases due to faults. Compared to FM4, it is known that M4 is more sensitive to low-order sidebands of the signal. Health indicators outlined in this section are represented by the following equations:

$$SER = \frac{\sum_{i=1}^{6} \left(A\left(f_{s(i)}\right) \right)}{A(f_1)} \tag{11}$$

$$FM4 = \frac{\frac{1}{N}\sum_{i=1}^{N}\left(DIF(i)-\mu_{DIF}\right)^4}{\left[\frac{1}{N}\sum_{i=1}^{N}\left(DIF(i)-\mu_{DIF}\right)^2\right]^2} \tag{12}$$

$$M4 = \frac{1}{N}\sum_{i=1}^{N}\left(RES(i)-\mu_{RES}\right)^4 \tag{13}$$

where N is the number of samples of the signal, $A(f_1)$ is amplitude of the fundamental gear meshing frequency (GMF, f_1), $A(f_{s(i)})$ is amplitude of the ith sidebands on each side of fundamental gear meshing frequency (f_1), $\mu_{(\cdot)}$ is the sample mean value of $(\bullet)$, $DIF(i)$ is ith sample of the difference signal, and $RES(i)$ is ith sample of the residual signal.

4. Case studies

This paper employs two case studies to demonstrate the effectiveness of ATSA: vibration signals generated by an analytical method and those measured from a wind turbine testbed. The vibration signal produced by the planet gear of interest is isolated from the noisy signals to be used for diagnostics of the planet gear.

It was stated in Section 1 that TSA requires stationary vibration signals under the rated operation of WTs. Even if vibration signals in rated operating condition of WTs could have a small amount of speed fluctuation, it is expected that their effects can be minimized by resampling vibration signal [23]. This paper, thus, employs the simulation and the test of the planetary gearbox ran for 100 min with the nominally constant rotational speed of 1600 rpm to the high-speed shaft. First, the operating data was divided into 100 data sets in which one minute of operating data is included. It corresponds to 393 carrier cycles of the gearbox. Second, the identical operating data was divided into 300 data sets so that each data set contains 131 carrier cycles of the gearbox. Signals from TSA with a Tukey window having five-tooth width, which is the most recently developed TSA for planetary gearboxes, are used for a comparison study.

4.1. Case study 1: simulation

4.1.1. Description of the simulation

An analytic vibration signal can be modeled using vibrations from the planet gear (v_p), and the non-coherent random noise (R):

$$v_a = \frac{1}{3}\sum_{i=1}^{3}\left(v_p a_{pi} + R\right) \tag{14}$$

where a_{pi} is the transfer factor that represents the relative distance of the ith planet gear from the sensor.

Planet gears in a gearbox theoretically produce the same amount of vibration energy (v_p) when simultaneously meshing with a ring gear. Therefore, the vibration signal from one planet gear (v_p) is defined as

$$v_p(t) = \cos\left(2\pi f_{rev} N_p t\right) \tag{15}$$

In this case study, it was assumed that the gearbox has three planet gears with 31 teeth and one sun gear. Although the three planet gears produce the same amount of vibration energy, the relative distance of each planet gear from a sensor affects the intensity of the signal measured by the sensor. The transfer factor of the ith planet gear (a_{pi}), thus, was designed and multiplied to the vibration produced by the ith planet gear, as shown in Fig. 13(a). When the planet gear approaches the sensor, the transfer factor gives greater weight. On the other hand, less weight is assigned when the planet gear recedes

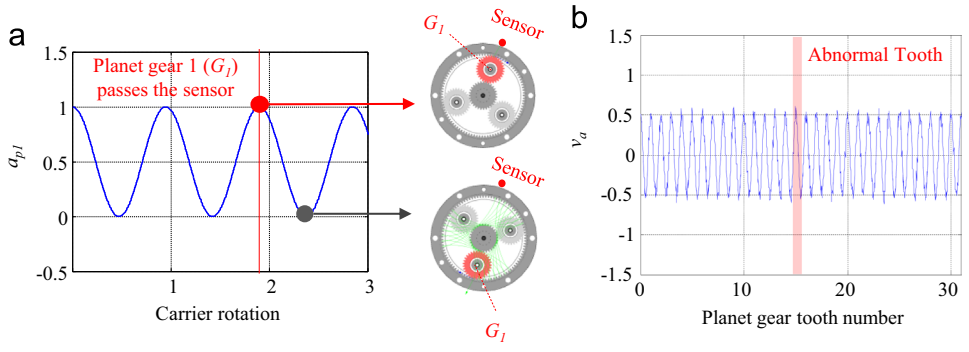

Fig. 13. Design of analytic signal: (a) transfer factor of planet 1 and (b) analytic signal.

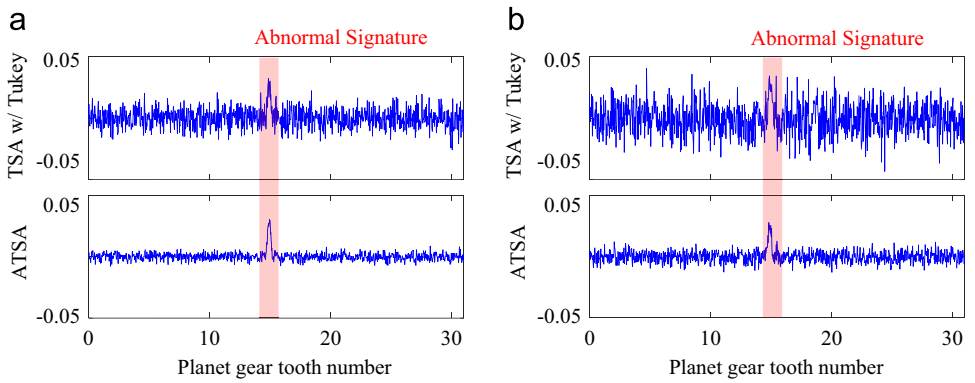

Fig. 14. *RES* of vibration signal produced by a planet gear from the simulation: (a) data length: 393 carrier cycles and (b) data length: 131 carrier cycles.

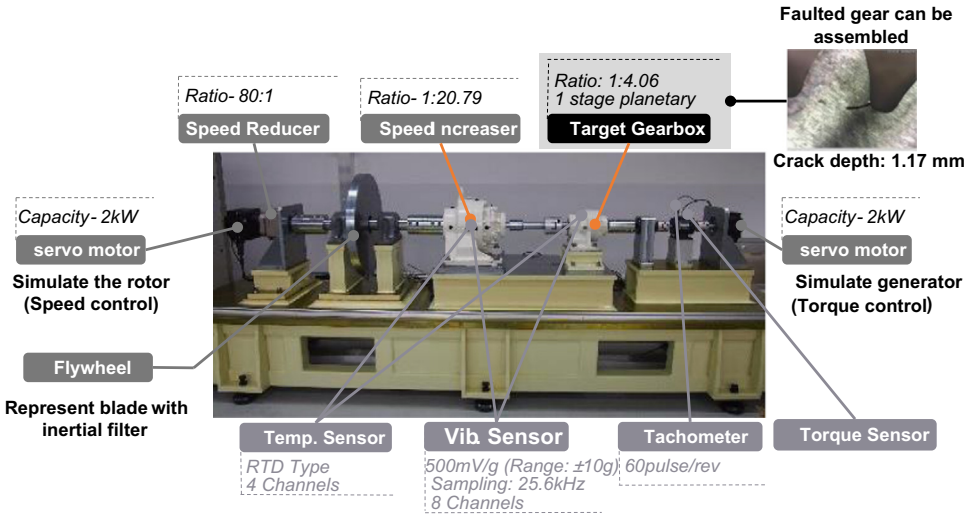

Fig. 15. Wind turbine testbed.

from the sensor. A fault was simulated in tooth number 14 on a planet gear by adding a half-period sine wave at instances when the faulty tooth of the planet gear contacted a tooth of the ring gear. This paper focuses only on the instances when the planet gear meshes with the ring gear under the sensor. Consequently, a faulty signal caused by contact between the faulty tooth of planet gear and the sun gear was not considered. In this study, a half-period sine wave with the amplitude of 0.1 was used to describe 10% of the amplitude of vibration signal from a planet gear. Non-coherent random noise (R) was also added to emulate many noise sources including measurement error, environmental noise, etc. It was designed to have a Gaussian distribution with a mean of zero and a standard deviation of 0.1. The standard deviation was set to be 10% of the amplitude of vibration signal from the planet gear. When all the factors were incorporated in the vibration signal, the effect of the faulty gear tooth was invisible in the tooth domain. It was buried by the background noise, as shown in Fig. 13(b).

4.1.2. Results

The simulated vibration signals were processed with the TSA and the developed ATSA. Then, *RES* and *DIF* of the processed signals were investigated. It was found that *RES* in the tooth domain was sufficient to figure out the abnormal signature. Fig. 14 compares two residual signals resulting from ATSA and conventional TSA with the Tukey window. Fig. 14(a and b) used the simulated vibration signals for 393 carrier cycles and 131 carrier cycles, respectively. Size of data (e.g., 393 and 131 carrier cycles) was determined to correspond with the case study with testbed. TSA with the Tukey window failed to show any abnormal signature in the case with operating data for 131 carrier cycles since the size of data was too limited to perform sufficient TSA processing with such a narrow-range window. An abnormal signature appeared when 393 carrier cycles of operating data were used for the TSA with the Tukey window. In contrast, ATSA results showed that it can detect an abnormal signature in both cases: operation data for 131 carrier cycles and also even more clearly for operation data for 393 carrier cycles.

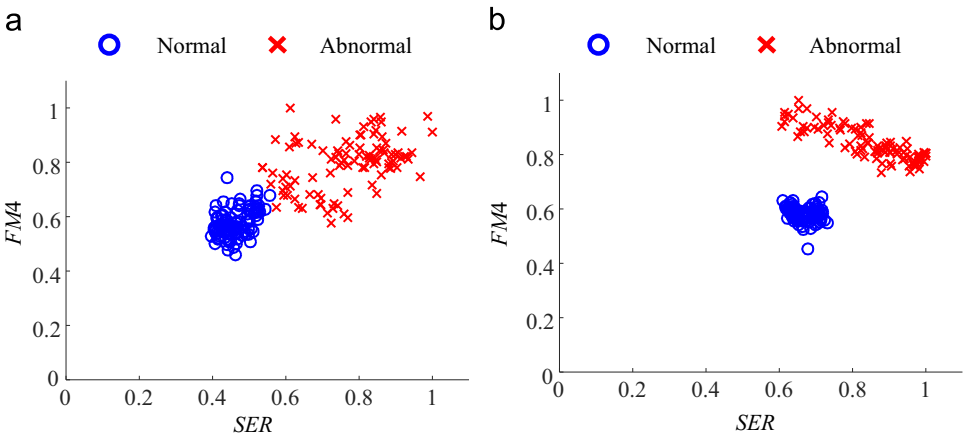

Fig. 16. Two health indicators (SER and FM4) using 393 carrier cycles of operational data measured from the WT testbed: (a) processed with TSA and (b) processed with ATSA.

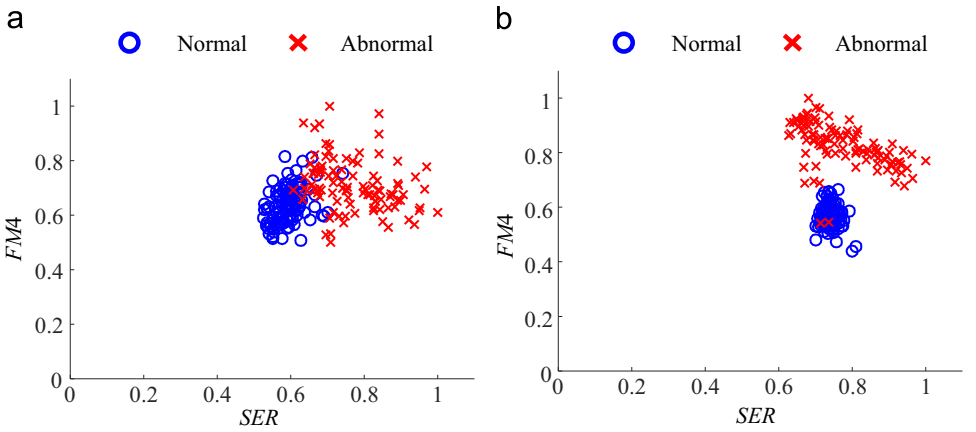

Fig. 17. Two health indicators (SER and FM4) using 131 carrier cycles of operational data measured from the WT testbed: (a) processed with TSA and (b) processed with ATSA.

4.2. Case study 2: testbed with 4:1 planetary gearbox

4.2.1. Description of the test

A 2 kW testbed was designed to emulate planetary gearboxes in WTs [24] as shown in Fig. 15. The testbed is comprised of two servo motors, a main bearing, a flywheel, gearboxes, and a measurement system with eight vibration sensors. The details of the testbed are available in [25]. The gearbox indicated in Fig. 15 was used to evaluate the performance of ATSA. The gearbox has one carrier, one ring gear with 95 teeth, one sun gear with 31 teeth and three planet gears with 31 teeth. Vibration data was acquired by the vibration sensor attached on the top of the planetary gearbox at 25.6 kHz of sampling rate. In this study, a planet gear with root crack was tested to evaluate the performance of ATSA because the surface damage of gears (e.g. wear) is known to be detected effectively through the oil/lubricant analysis [26]. For design of realistic curved shape of the crack, crack propagation was estimated by tracing the path that achieves maximum stress intensity at the crack tip with the use of finite element model of the gear. In addition, the critical crack length was defined in such a way that the stress intensity at the crack tip reached the fracture toughness of the gear with the safety factor of 20. As a conservative approach, the safety factor was set to be twice the value used for certifying wind turbines [27], accounting for the guideline about the safety factor of root bending for gears in power transmission systems [28]. As a result, a curved crack with the depth of 1.17 mm was designed and artificially seeded by wire electric discharge cutting at the tooth root of the planet gear. Then, the faulty gear was re-assembled into the gearbox to emulate abnormal condition.

4.2.2. Results

This case study employed the three health indicators (i.e. *SER*, *FM4*, and *M4*) to detect the signature generated by the faulty planetary gear. The signals in the tooth domain were not presented since the analysis of *RES* and *DIF* did not show any signature associated with the crack because of the large amount of noise from uncertainties of the testbed. In Figs. 16 and 17, a comparison of the results using Tukey-based TSA and ATSA is presented using *M4* and *SER*. Each data point represents

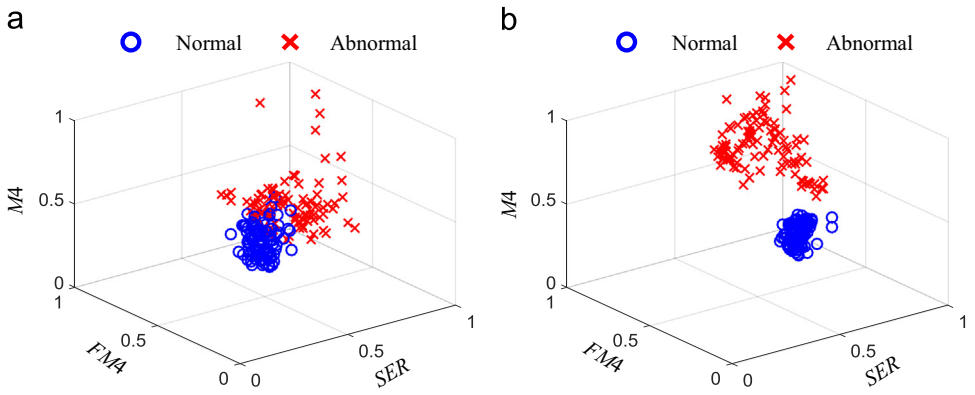

Fig. 18. Three health indicators (SER, FM4 and M4) using 131 carrier cycles of operational data measured from the WT testbed: (a) processed with TSA and (b) processed with ATSA.

health indicator processed with Tukey-based TSA and ATSA for which 393 carrier cycles or 131 carrier cycles of operational data were used. As shown in Figs. 16 and 17, the health indicators from the abnormal condition represent the large magnitude and variation compared to those from the normal condition, as can be inferred from the definition of the health indicators. When a sufficient amount of data is available (e.g., 393 carrier cycles), in Fig. 16, health indicators processed with ATSA can clearly differentiate the normal condition from the abnormal condition whereas HIs processed with TSA are uncertain, at best. When the available data is limited (e.g., 131 carrier cycles), HIs from TSA failed to differentiate the normal condition and the abnormal condition of the gearbox, whereas HIs from ATSA could mostly did as shown in Fig. 17. However, ATSA were still not able to perfectly differentiate the normal condition and the abnormal condition with only two HIs. When one more health indicator (M4) is employed, it can be shown in Fig. 18 that ATSA effectively distinguished the normal condition from the abnormal condition with the limited amount of data whereas TSA could not do.

5. Conclusions

The autocorrelation-based time synchronous averaging (ATSA) method was proposed as an improved pre-processing technique for fault diagnosis of planetary gearboxes. Autocorrelation analysis of the vibration signal was performed to identify the instances when a similar pattern of vibration occurred. A window function with an optimized size and shape was designed based on the autocorrelation function to overcome the limitations of the narrow-range and full-range windows. It was demonstrated that, using the simulated vibration signals, ATSA with the newly designed window function outperformed the Tukey window-based TSA in identifying a fault signature in the tooth domain. Another case study was performed by employing 393 and 131 carrier cycles of operational data, which corresponded to 19.65 and 6.55 min of operation of a typical wind turbine operating at 20 rpm at the blade. It was verified that TSA is feasible when the available data is sufficient (e.g., 19.65 min of stationary operation). However, such a long time period of stationary operation rarely happens in a wind turbine. Therefore, it is reasonable to conclude that ATSA is an efficient pre-processing technique for diagnostics of gearboxes in WTs, especially where the amount of available stationary data is limited (e.g., less than 7 min of operation), where conventional TSA is not feasible. With the signal processed with ATSA, effectiveness of any kinds of works related to condition monitoring of the gear, such as fault alarming, fault diagnostics, prognostics, etc. can be enhanced significantly compared to the methods with the conventional TSA.

6. Future works

We identified several pieces of future work to make the propose ATSA method be applicable to the fault diagnostics of actual gearboxes in WTs which are subjected to the various environmental and operating conditions. Firstly, the performance of the ATSA should be verified with data that contain a large amount of speed fluctuation. From this verification, it would also be possible to identify what amount of speed fluctuation TSA is applicable without any other advanced signal processing techniques. Secondly, various types of faults (e.g. surface damage) should be tested to demonstrate the performance of the ATSA in the reliable classification of various faults. Thirdly, it is desirable to evaluate the robustness of ATSA using field data collected from various operating conditions in real-world applications. Fourth, it is required to employ an advanced signal processing technique (e.g. time-frequency analysis) for condition monitoring of WTs in non-stationary operation. Lastly, the data size should be effectively managed by (1) reduction of sampling rate and (2) identification of useless data for data reduction.

Acknowledgments

This work was partially supported by the two research projects of the International Collaborative Energy Technology R&D Program of the Korea Institute of Energy Technology Evaluation and Planning (KETEP) granted financial resource from the Ministry of Trade, Industry & Energy, Republic of Korea (No. 20118520020010) and Mid-career Researcher Program through the National Research Foundation of Korea (NRF) grant funded by the Ministry of Science ICT and Future Planning (MSIP) (2013R1A2A2A01068627).

References

[1] F.P. García Márquez, A.M. Tobias, J.M. Pinar Pérez, M. Papaelias, Condition monitoring of wind turbines: techniques and methods, Renew. Energy 46 (2012) 169–178.
[2] S. Sheng, Investigation of various condition monitoring techniques based on a damaged wind turbine gearbox, In: Proceedings of 8th International Workshop on Structural Health Monitoring, Stanford, California, 2011.
[3] B. Lu, Y. Li, X. Wu, Z. Yang, A review of recent advances in wind turbine condition monitoring and fault diagnosis, In: Proceedings of the Power Electronics and Machines in Wind Applications (PEMWA) 2009, IEEE, Lincoln, NE, 2009, pp. 1–7.
[4] Germanischer Lloyd (GL), Rules and Guidelines Industrial Services Part 4 – Guideline for the Certification of Condition Monitoring Systems for Wind Turbines, Germanischer Lloyd (GL), 2013.
[5] P.D. McFadden, A revised model for the extraction of periodic waveforms by time domain averaging, Mech. Syst. Signal Process. 1 (1987) 83–95.
[6] A.K.S. Jardine, D. Lin, D. Banjevic, A review on machinery diagnostics and prognostics implementing condition-based maintenance, Mech. Syst. Signal Process. 20 (2006) 1483–1510.
[7] P.D. McFadden, I.M. Howard, The Detection of Seeded Faults in an Epicyclic Gearbox by Signal Averaging of the Vibration, AR-006-087/ARL-PROP-R-183, Commonwealth of Australia, 1990.
[8] P.D. McFadden, Window functions for the calculation of the time domain averages of the vibration of the individual planet gears and sun gear in an epicyclic gearbox, J. Vib. Acoust. 116 (1994) 179–187.
[9] P.D. Samuel, J.K. Conroy, D.J. Pines, Planetary Transmission Diagnostics, NASA/CR-2004-213068, NASA Glenn Research Center, 2004.
[10] V.A. Hines, A.B. Ogilvie, C.R. Bond, Continuous Reliability Enhancement for Wind (CREW) Database: Wind Plant Reliability Benchmark, Sandia National Laboratories, 2013.
[11] B.D. Forrester (Inventor, Aeronautical and Martime Research Laboratory, assignee). Method for the Separation of Epicyclic Planet Gear Vibration Signatures, United States Patent US 6,298,725 B1, 2001.
[12] P.D. McFadden, Interpolation techniques for time domain averaging of gear vibration, Mech. Syst. Signal Process. 3 (1989) 87–97.
[13] A. Hood, P. Darryll, Sun gear fault detection on an OH-58C helicopter transmission, in: American Helicopter Society 67th Annual Forum, American Helicopter Society, 2011, pp. 1664–1690.
[14] P.D. McFadden, A technique for calculating the time domain averages of the vibration of the individual planet gears and the sun gear in an epicyclic gearbox, J. Sound Vib. 144 (1991) 163–172.
[15] D.G. Lewicki, R.T. Ehinger, J. Fetty, Planetary gearbox fault detection using vibration separation techniques, NASA/TM—2011-217127, NASA Glenn Research Center, 2011.
[16] M.R. de Smidt, Internal Vibration Monitoring of a Planetary Gearbox, Master of Engineering, Department of Mechanical and Aeronautical Engineering, University of Pretoria, 2009.
[17] J. Yu, Early fault detection for gear shaft and planetary gear based on wavelet and hidden markov modeling (Ph.D. thesis), Department of Mechinical and Industrial Engineering, University of Toronto, 2011.
[18] M. Lebold, K. Mcclintic, R. Campbell, C. Byington, K. Maynard, Review of vibration analysis methods for gearbox diagnostics and prognostics, In: Proceedings of the 54th Meeting of the Society for Machinery Failure Prevention Technology, Virginia Beach, 2000, pp. 623–634.
[19] P.D. McFadden, Examination of a technique for the early detection of failure in gears by signal processing of the time domain average of the meshing vibration, Mech. Syst. Signal Process. 1 (1987) 173–183.
[20] P.D. Samuel, D.J. Pines, A review of vibration-based techniques for helicopter transmission diagnostics, J. Sound Vib. 282 (2005) 475–508.
[21] S. Sheng, Wind Turbine Gearbox Condition Monitoring Round Robin Study – Vibration Analysis, Technical Report NREL/TP-5000-54530, National Renewable Energy Laboratory (NREL), 2012.
[22] R.M. Stewart, Some Useful Data Analysis Techniques for Gearbox Diagnostics, Technical Report MHM/R/10/77, Machine Health Monitoring Group, Institute of Sound and Vibration Research, University of Southampton, 1977.
[23] N. Ahamed, Y. Pandya, A. Parey, Spur gear tooth root crack detection using time synchronous averaging under fluctuating speed, Measurement 52 (2014) 1–11.
[24] K. Oh, J. Lee, H. Bang, J. Park, J. Lee, B.I. Epureanu, Development of a 20 kW wind turbine simulator with similarities to a 3 MW wind turbine, Renew. Energy 62 (2014) 379–387.
[25] J.M. Ha, Vibration-Based Framework for Fault Diagnostics of Wind Turbine Gearbox, Master of Science, Department of Mechanical and Aerospace Engineering, Seoul National University, 2013.
[26] M. Kumar, P.S. Mukherjee, N.M. Misra, Advancement and current status of wear debris analysis for machine condition monitoring: a review, Ind. Lubr. Tribol. 65 (2013) 3–11.
[27] International Electrotechnical Commission (IEC), Wind Turbine—Part 1: Design Requirements, IEC 61400-1, International Electrotechnical Commission, 2005.
[28] Korean Register of Shipping, Rules for the classification of steel ships, Korean Register of Shipping, 1980.